Explicit inclusion of the spin-orbit contribution in the Tohsaki-Horiuchi-Schuck-Röpke wave function

N. Itagaki,[1] H. Matsuno,[2] and A. Tohsaki[3]

[1]*Yukawa Institute for Theoretical Physics, Kyoto University, Kitashirakawa Oiwake-Cho, Kyoto 606-8502, Japan*
[2]*Department of Physics, Kyoto University, Kitashirakawa Oiwake-Cho, Kyoto 606-8502, Japan*
[3]*Research Center for Nuclear Physics, 10-1 Mihogaoka, Ibaraki, Osaka 067-0047, Japan*

The Tohsaki-Horiuchi-Schuck-Röpke (THSR) wave function has been successfully used for the studies of gaslike nature of α clusters in various nuclei, including the so-called Hoyle state of ^{12}C and four α states of ^{16}O. In standard α cluster models, however, each α cluster wave function has spin zero because of its spatial symmetry and antisymmetrization effect. Thus the noncentral interactions do not contribute, and this situation is the same in the THSR wave function. In this work, the spin-orbit contribution, which is found to be quite important at short α-α distances, is taken into account in the THSR wave function by combing it with antisymmetrized quasicluster model (AQCM). The application to ^{12}C is presented. The multi-integration in the original THSR wave function is carried out by using a Monte Carlo technique, which is called the Monte Carlo THSR wave function. For the nucleon-nucleon interaction, the Tohsaki interaction, which contains finite-range three-body terms and simultaneously reproduces the saturation properties of nuclear systems, the α-α scattering phase shift, and the size and binding energy of ^{4}He, is adopted.

I. INTRODUCTION

The Tohsaki-Horiuchi-Schuck-Röpke (THSR) wave function has been widely used for the studies of gaslike states of α clusters, including the so-called Hoyle state of ^{12}C and four α states of ^{16}O [1,2]. In normal α cluster models, each α cluster is described by Gaussian-type wave function, and the positions of the α clusters are specified by Gaussian center parameters. In the THSR framework, all of these Gaussian center parameters are integrated out with a weight function, which enables us to describe well-extended cluster states. Also, by choosing a small range for the weight function, the lowest configuration of the harmonic oscillator shell model is described. Recently, a "container picture" has been proposed for the description of nonlocalized clusters [3], and also the framework has been applied even to nuclei such as ^{9}Be, etc., which do not belong to $4N$ nuclei [4].

One of the problems of the traditional cluster models is that the noncentral interactions, especially the spin-orbit interaction, which is quite important in explaining the observed magic numbers, do not contribute; they work neither inside α clusters nor between α clusters. In cluster models, each α cluster is often defined as a simple $(0s)^4$ configuration at some spatially localized point. In this case, the antisymmetrization effect automatically makes the α cluster a spin singlet system where noncentral interactions do not contribute. To include the spin-orbit contribution starting with the cluster model, we proposed the antisymmetrized quasicluster model (AQCM) [5–14]. This method allows us to smoothly transform α cluster model wave functions to jj-coupling shell model ones, and we call the clusters that feel the spin-orbit effect after this treatment quasiclusters. In AQCM, we have

only two parameters: R representing the distance between α clusters and Λ characterizing the transition of α cluster(s) to quasicluster(s). It has been known that the conventional α cluster models cover the model space of closure of major shells ($N = 2$, $N = 8$, $N = 20$, etc.) of the jj-coupling shell model. In addition, we have shown that the subclosure configurations of the jj-coupling shell model, $p_{3/2}$ ($N = 6$), $d_{5/2}$ ($N = 14$), $f_{7/2}$ ($N = 28$), and $g_{9/2}$ ($N = 50$) that arise from the one-body spin-orbit interaction of the mean-field can be reasonably described by our AQCM [11].

For such calculations, which include both cluster and shell features, we inevitably need a reliable nucleon-nucleon interaction, not cluster-cluster interaction. It is quite well known that the central part of the interaction should have proper density dependence in order to satisfy the saturation property of nuclear systems. If we just introduce a simple two-body interaction, for instance, the Volkov interaction [15], which has been widely used in cluster studies, we have to choose a proper Majorana exchange parameter for each nucleus, and consistent description of two different nuclei with the same Hamiltonian becomes almost impossible. Adding a zero-range three-body interaction term helps to get better agreement with experiments; however, the radius and binding energy of free ^{4}He (α cluster) are not well reproduced [16]. The Tohsaki interaction, which has finite range three-body terms, has many advantages [5,17,18]. Although this is a phenomenological interaction, it gives reasonable size and binding energy of the α cluster, and α-α scattering phase shift is reproduced, while the saturation properties of nuclear matter are also reproduced rather sufficiently.

In this paper, we combine the THSR wave function and the idea of AQCM. It is worthwhile to show the applicability of the combined method by numerical calculations. The THSR wave function contains the multi-integration over the Gaussian center parameters of α clusters, and this procedure can be numerically performed using a Monte Carlo technique called the Monte Carlo THSR wave function [19–23]. In the present study, we calculate ^{12}C (three α) as the first step. The ground state of ^{12}C corresponds to the subclosure configuration of jj-coupling shell model, and breaking α clusters is quite important. Recently various kinds of microscopic approaches have shown the importance of the mixing of shell and cluster components, and transition strengths, α-decay widths, and scattering phenomena have been discussed [24–35]. Some of these approaches are modern *ab initio* ones and even the tensor and short-range correlations are included. Compared with these, our approach is rather phenomenological, but here we examine the natural extension of the THSR framework and include the spin-orbit correlation.

II. FRAMEWORK

In this section, we summarize the essence of the THSR wave function and AQCM, and the combination of these two is newly introduced.

A. Brink model

The THSR wave function is based on the Brink model [36]. Each single-particle wave function of the Brink model is described by a Gaussian,

$$\phi_{ij} = \left(\frac{2\nu}{\pi}\right)^{\frac{3}{4}} \exp[-\nu(\boldsymbol{r}_j - \boldsymbol{R}_i)^2]\chi_j, \tag{1}$$

where the Gaussian center parameter $\boldsymbol{R}_i$ shows the expectation value of the position of the ith α cluster. The index j specifies four nucleons in this ith α cluster, and χ_j represents the spin isospin part of the single-particle wave function. The size parameter ν is chosen to be $0.25 \, \text{fm}^{-2}$, which reproduces the observed radius of ^{4}He.

The Slater determinant of the Brink model is constructed from these single-particle wave functions by antisymmetrizing them. Here, four single-particle wave functions with different spin and isospin sharing a common Gaussian center parameter correspond to an α cluster:

$$\Phi_{SD}(\boldsymbol{R}_1, \boldsymbol{R}_2, \ldots, \boldsymbol{R}_N) = \mathcal{A}\{(\phi_{11}\phi_{12}\phi_{13}\phi_{14})(\phi_{21}\phi_{22}\phi_{23}\phi_{24})$$
$$\cdots (\phi_{N1}\phi_{N2}\phi_{N3}\phi_{N4})\}. \tag{2}$$

This is the case in which we have N α clusters and the mass number A is equal to $A = 4N$.

B. THSR wave function

The idea of the THSR wave function [1] is that Gaussian center parameters $\{\boldsymbol{R}_i\}$ are integrated over infinite space with the weight functions $\{\exp[-\boldsymbol{R}_i^2/\sigma^2]\}$. Thus the THSR wave

function Φ_{THSR} is expressed using Φ_{SD} in Eq. (2) as

$$\Phi_{\text{THSR}} = \int d\boldsymbol{R}_1 d\boldsymbol{R}_2 \cdots d\boldsymbol{R}_N \, \Phi_{SD}(\boldsymbol{R}_1, \boldsymbol{R}_2, \ldots, \boldsymbol{R}_N)$$
$$\times \exp\left[-\left(\boldsymbol{R}_1^2 + \boldsymbol{R}_2^2 + \cdots + \boldsymbol{R}_N^2\right)/\sigma^2\right]. \tag{3}$$

Here σ is a control parameter, which governs the spatial extension of the system. When σ is larger than $1/\nu$, the wave function describes gaslike states of α clusters, and the lowest configuration of the harmonic oscillator shell model can be realized at the limit of $\sigma \to 0$.

C. Monte Carlo THSR

In some cases of the original THSR wave function, the analytic formula for the matrix elements for the Hamiltonian is already obtained. However for heavier nuclei, it is useful to introduce a Monte Carlo technique for the multi-integration in the original THSR wave function [19–23]. We call this wave function ($\Phi_{\text{M-THSR}}$) Monte Carlo THSR:

$$\Phi_{\text{M-THSR}} = \sum_k^{N_{\text{max}}} P^{J^\pi} \Phi_{SD}\left(\boldsymbol{R}_1^k, \boldsymbol{R}_2^k, \ldots, \boldsymbol{R}_N^k\right). \tag{4}$$

Here the multi-integration over the Gaussian center parameters in Eq. (3) is replaced with a summation of different Slater determinants. The Slater determinants superposed have different values of Gaussian center parameters $\{\boldsymbol{R}_i^k\}$ for N α clusters, where k is a number to specify the set of the Gaussian center parameters for the kth Slater determinant. The value of the Gaussian center parameters are randomly generated, but the distribution of the absolute value $|\boldsymbol{R}_i^k|$ for the ith α cluster is introduced to be proportional to $\exp[-(\boldsymbol{R}_i^k/\sigma)^2]$, and its angular part is isotropically generated. Thus the information of the weight function in the original THSR wave function is absorbed in the distribution of randomly generated $\{\boldsymbol{R}_i^k\}$ values. The value of N_{max} shows the number of Slater determinants, which are superposed. The limit of $N_{\text{max}} \to \infty$ coincides with the original THSR wave function; however, we approximate it with a finite number. In Eq. (4), P^{J^π} shows the projection onto the eigenstates of parity and angular momentum, and this is numerically performed.

D. AQCM

In the conventional cluster models, there is no spin-orbit effect for the α clusters. Thus they are changed into quasiclusters based on AQCM [5–14]. According to AQCM, when the original position of one of the α clusters (the value of Gaussian center parameter) is $\boldsymbol{R}$, the Gaussian center parameter of the lth nucleon in this cluster is transformed by adding the imaginary part as

$$\boldsymbol{\zeta}_l = \boldsymbol{R} + i\Lambda\boldsymbol{e}_l^{\text{spin}} \times \boldsymbol{R}, \tag{5}$$

where $\boldsymbol{e}_l^{\text{spin}}$ is a unit vector for the intrinsic-spin orientation of the lth nucleon in this α cluster. For the imaginary part we introduce Λ, which is a real dimensionless parameter. After this transformation, this α cluster is called a quasicluster. The imaginary part, which is added, depends on the spin direction of each nucleon, thus the α cluster is no longer a spin

singlet system. The spin-orbit contribution can be taken into account by this transformation, and the spin-orbit contribution is attractive (negative in energy) when Λ is positive. We have previously shown that the lowest configurations of the jj-coupling shell model can be achieved by $\Lambda = 1$ and $\boldsymbol{R} \to 0$.

E. Monte Carlo THSR + AQCM

We propose a new framework by combining Monte Carlo THSR and AQCM, which is applied to ^{12}C. For ^{12}C, we introduce AQCM for all the three α clusters. Here the intrinsic spins of the nucleons in the three α clusters are introduced to have threefold symmetry. This is needed to include the lowest configuration of the jj-coupling shell model (subclosure configuration of $p_{3/2}$) within a single Slater determinant. In the first α cluster, each intrinsic-spin of the four nucleons is spin-up (z direction) for a proton and a neutron and spin-down ($-z$ direction) for a proton and a neutron. The intrinsic-spin orientations of the four nucleons in the second and third α clusters are introduced by rotating the ones of the first α cluster by $2\pi/3$ and $4\pi/3$ radians, respectively. These spin orientations of the twelve nucleons are fixed in all Slater determinants before angular momentum projection. While fixing the intrinsic-spin orientations, at first we randomly generate the center parameters of three α clusters based on Monte Carlo TSHR and shift their sum to the origin, $\sum_i \vec{R}_i^k = 0$. Finally, imaginary parts of the Gaussian center parameters are introduced based on AQCM as in Eq. (5), and angular momentum projection and superposition of different Slater determinants follow. Here the second step of shifting the center of mass to the origin is quite important; the purpose of AQCM treatment is to describe the single-particle motion of each nucleon around the origin and take into account the spin-orbit contribution, thus the center of the nucleus has to coincide with the origin of the coordinate system before giving the imaginary part.

F. Hamiltonian

The Hamiltonian ($\hat{H}$) consists of kinetic energy ($\hat{T}$) and potential energy ($\hat{V}$) terms, and the kinetic energy term is described as one-body operator,

$$\hat{T} = \sum_i \hat{t}_i - T_{\text{cm}}, \qquad (6)$$

and the center of mass kinetic energy (T_{cm}), which is constant given by the size parameter ν, is subtracted. The potential energy has central, spin-orbit, and Coulomb parts. For the central part, we introduce the Tohsaki interaction [17], which has finite range three-body terms in addition to the two-body nucleon-nucleon interaction terms. This interaction is designed to reproduce both the saturation property and the scattering phase shift of two α clusters. We use the F1 parameter set [17] in the present analysis, which was used in the original THSR work for ^{12}C.

For the spin-orbit part ($\hat{V}_{\text{so}}$), the spin-orbit term of G3RS [37], which is a realistic interaction originally determined to reproduce the nucleon-nucleon scattering phase shift, is
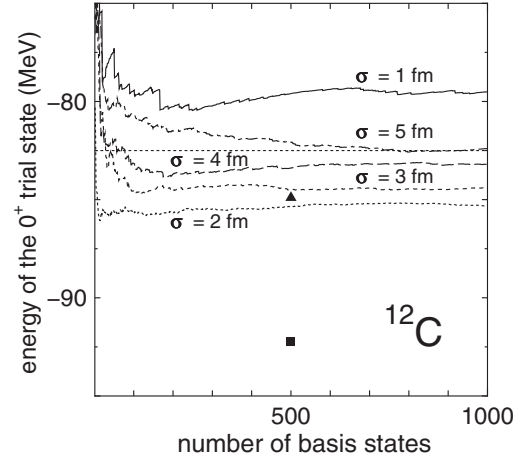

FIG. 1. The 0^+ energy convergence of ^{12}C [three α's] as a function of the number of Slater determinants superposed [N_{max} in Eq. (4)] calculated with the Monte Carlo THSR framework. The α clusters are not broken [$\Lambda = 0$ in Eq. (5)], and the solid, dotted, short-dashed, dashed, and dash-dotted lines correspond to $\sigma = 1$, 2, 3, 4, and 5 fm in Eq. (3), respectively. The dashed line at -82.50 MeV shows the calculated three-α threshold energy. The solid square at -92.2 MeV and the solid triangle at -84.9 MeV show the experimental values for energies of the ground state and three-α threshold, respectively.

adopted:

$$\hat{V}_{\text{so}} = \sum_{i<j} V_{ls} \left(e^{-d_1(\boldsymbol{r}_i - \boldsymbol{r}_j)^2} - e^{-d_2(\boldsymbol{r}_i - \boldsymbol{r}_j)^2} \right) P(^3O) \boldsymbol{L}_{ij} \cdot \boldsymbol{S}_{ij},$$
$$(7)$$

where $d_1 = 5.0\,\text{fm}^{-2}$, $d_2 = 2.778\,\text{fm}^{-2}$, and $P(^3O)$ is a projection operator onto a triplet odd state. The operator $\boldsymbol{L}_{ij}$ stands for the angular momentum for the relative coordinate $(\boldsymbol{r}_i - \boldsymbol{r}_j)$, and $\boldsymbol{S}_{ij}$ is the total spin ($\boldsymbol{S}_{ij} = \boldsymbol{S}_i + \boldsymbol{S}_j$). The strength, V_{ls}, has been determined to reproduce the ^{4}He $+ n$ scattering phase shift [38], and $V_{ls} = 1600$–2000 MeV has been suggested. Here we employ $V_{ls} = 1800$ MeV, which has been tested in our previous works for ^{12}C [5], although there the Majorana parameter for the three-body (central) interaction is slightly modified to reproduce the binding energy of ^{16}O.

III. RESULTS AND DISCUSSIONS

We start the Monte Carlo THSR calculation with the α nonbreaking case, which is nothing but the superposition of Brink-type α cluster model wave functions. In the AQCM framework, this situation corresponds to setting Λ in Eq. (5) to zero. In Fig. 1, the 0^+ energy convergence of ^{12}C (three α clusters) is shown as a function of the number of Slater determinants superposed in the Monte Carlo THSR framework [N_{max} in Eq. (4)]. The solid, dotted, short-dashed, dashed, and dash-dotted lines correspond to $\sigma = 1$, 2, 3, 4, and 5 fm in Eq. (3), respectively. The dashed line at -82.50 MeV shows the three-α threshold energy. The solid square at -92.2 MeV and the solid triangle at -84.9 MeV show the experimental values for energies of the ground state and three-α
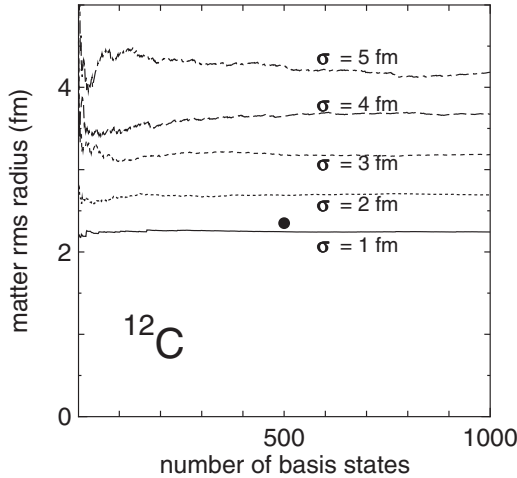
FIG. 2. The convergence of the root mean square (rms) matter radius for the 0^+ state of ^{12}C as a function of the number of Slater determinants superposed [N_{max} in Eq. (4)] calculated with the Monte Carlo THSR framework. The α clusters are not broken [Λ in Eq. (5) is zero], and the solid, dotted, short-dashed, dashed, and dash-dotted lines correspond to $\sigma = 1, 2, 3, 4$, and 5 fm in Eq. (3), respectively. The solid circle at 2.35 fm shows the experimental value for the ground state deduced in Ref. [39].

FIG. 3. The 0^+ energy curve of ^{12}C as a function of σ defined in Eq. (3). The dotted line is for $\Lambda = 0$. The solid line is obtained when Λ is taken as a variational parameter to minimize the energy. The values in the parentheses show the optimal Λ values for the cases of $\sigma = 1.0, 2.0$, and 3.0 fm. The dashed line at -82.50 MeV shows the calculated three-α threshold energy. The solid square at -92.2 MeV and the solid triangle at -84.9 MeV show the experimental values for energies of the ground state and three-α threshold, respectively.

threshold, respectively. This is a Monte Carlo calculation and not variational one, thus the energy is not always going down; the energy sometimes goes up with increasing number of the basis states. Nevertheless, the energy converges at the limit of $N_{max} \to \infty$, but here we can confirm that it is well converged with 1000 basis states [$N_{max} = 1000$ in Eq. (4)]. In this calculation, the radial parts of the Gaussian center parameters $\{R_i\}^k$ are generated by the random numbers $\{r_i\}$, whose distribution is proportional to $\exp[-r_i^2/\sigma^2]$, and the angular part of each R_i is isotropically generated using random numbers. It is found that the converged energy of the small-σ case, $\sigma = 1$ fm (solid line), is above the three-α threshold. This is because the contribution of the spin-orbit interaction, which is important in inner regions, is missing within the $\Lambda = 0$ wave functions. Other σ values give the energies below the threshold, and the dotted line ($\sigma = 2$ fm) gives the lowest energy. With increasing σ value, the energy again goes up, and the energy of $\sigma = 5$ fm (dash-dotted line) is close to the threshold.

Using these wave functions, the convergence of the root mean square (rms) matter radius for the 0^+ states of ^{12}C is shown in Fig. 2. The basis states are the same as those in Fig. 1, the wave functions are $\Lambda = 0$ (Brink α cluster model), and the types of the lines are also the same; the solid, dotted, short-dashed, dashed, and dash-dotted lines correspond to $\sigma = 1, 2, 3, 4$ and 5 fm in Eq. (3), respectively. Experimentally the rms matter radius of ^{12}C is obtained as 2.35(2) fm in Ref. [39], consistent with the value deduced from the electron scattering (solid circle in Fig. 2). The trial state, which gives the lowest energy within $\Lambda = 0$, is $\sigma = 1$ fm in the case of this interaction, and this states gives a slightly larger rms radius than the experiment. However the energy of the trial state as a function of σ changes drastically if we incorporate
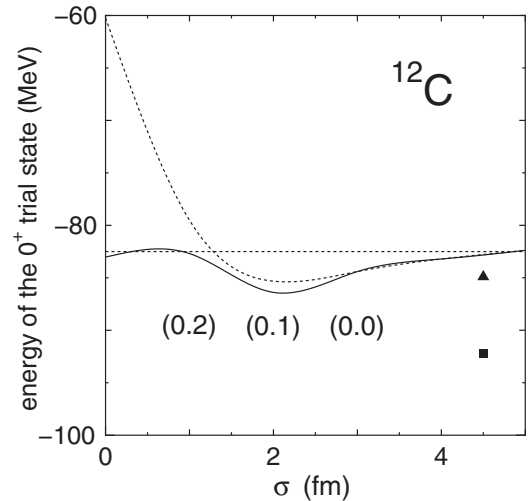
the spin-orbit effect as we discuss below. For the second 0^+ state known as the Hoyle state, the large rms radius of ~4.0 fm has been extensively discussed, although this state is a resonance state slightly above the threshold and the experimental determination is difficult. In the present case, the $\sigma = 5$ fm result (dash-dotted line) gives an energy around the threshold and an rms radius of 4.18 fm.

Then we take finite Λ values, which allows us to take into account the spin-orbit contribution. The energy of the 0^+ trial state for ^{12}C is shown in Fig. 3 as a function of σ. The solid line depicts the energy of the trial state when Λ is a variational parameter, while $\Lambda = 0$ for the dotted line. For the solid line, the values in the parentheses show the optimal Λ values for the cases of $\sigma = 1.0, 2.0$, and 3.0 fm. After optimizing the value for Λ we can see in the limit $\sigma = 0$ a drastic increase in binding due to a large contribution of the spin-orbit interaction, and $\sigma = 0$ fm becomes a local minimum point of the solid line. The optimal Λ value of 0.3 at the limit of $\sigma = 0$ fm means that the α clusters are broken to some extent and the wave function approaches to the jj-coupling shell model one. In general, the contribution of the spin-orbit interaction increases and the energy decreases with increasing Λ (for each fixed σ), but it saturates at some point because the kinetic energy grows with the square of Λ.

As a function of σ, in Fig. 3, the energy minimum point of the solid line appears around $\sigma = 2.0$ fm, where the optimal Λ value is 0.1. Owing to the additional attraction of the spin-orbit interaction, here the solid line is lower than the dotted line by about 1 MeV. We can superimpose the trial states at the two minima, absolute minimum at ($\sigma = 2.0$ fm, $\Lambda = 0.2$) and local minimum at ($\sigma = 0$ fm, $\Lambda = 0.3$), and obtain the mixing amplitude by diagonalizing the Hamiltonian based on
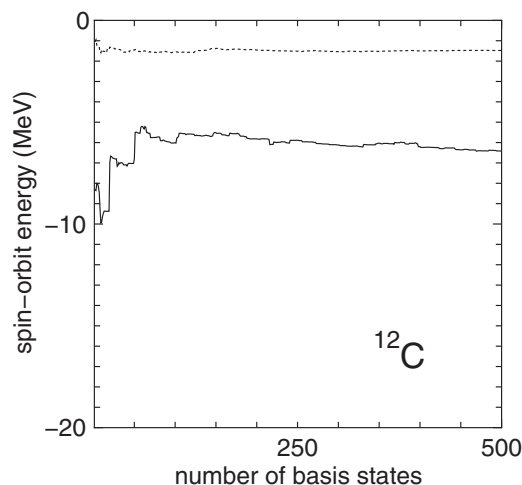
FIG. 4. The convergence of the spin-orbit energy for the 0^+ state of ^{12}C as a function of number of Slater determinants superposed [N_{max} in Eq. (4)]. The solid line is for $\sigma = 1.0$ fm and $\Lambda = 0.2$, and the dotted line is for $\sigma = 2.0$ fm and $\Lambda = 0.1$.

FIG. 5. The contribution of three-body interaction terms for the 0^+ state of ^{12}C as a function of the number of Slater determinants superposed [N_{max} in Eq. (4)] calculated with the Monte Carlo THSR framework. The σ value defined in Eq. (3) is 2.0 fm, and Λ in Eq. (5) is 0.1 (solid line) and 0 (dotted line).

the generator coordinate method (GCM). The energy becomes -87.5 MeV, lower than the value of ($\sigma = 2.0$ fm, $\Lambda = 0.2$) by more than 1.1 MeV, and the rms matter radius becomes 2.37 fm, which reproduces the experimental value.

The convergence of the spin-orbit energy for the 0^+ state of ^{12}C is shown in Fig. 4 as a function of number of Slater determinants superposed [N_{max} in Eq. (4)]. This is a demonstration that the spin-orbit effect can be successfully taken into account with the procedure proposed here. The solid line is for ($\sigma = 1.0$ fm, $\Lambda = 0.2$), and the dotted line is for ($\sigma = 2.0$ fm, $\Lambda = 0.1$). The Λ values are optimal ones in each σ case, and the latter gives the lowest energy point in Fig. 4. The solid line ($\sigma = 1.0$ fm, $\Lambda = 0.2$) converges to ~ -6.4 MeV, whereas the dotted line ($\sigma = 2.0$ fm, $\Lambda = 0.1$) converges to ~ -1.5 MeV.

After introducing nonzero Λ values, each nucleon is more independently treated and calculation costs significantly increase compared with the Brink model ($\Lambda = 0$) calculation. Therefore, in Fig. 3, although the contribution of the kinetic energy is calculated with superposing 1000 Slater determinants [$N_{max} = 1000$ in Eq. (4)], the contribution of the two-body interactions is estimated with 500 Slater determinants [$N_{max} = 500$]. The most time-consuming part is the finite-range three-body interaction part. This three-body part is substituted with the values obtained with the $\Lambda = 0$ wave functions. The three-body interaction terms do not strongly depend on the Λ values, and we can approximate it with the Brink model. The Brink model calculation is rather simple, and we can superpose 1000 basis states for the estimation of the three-body terms. This approximation can be justified in Fig. 5, which shows the contribution of the three-body interaction. The σ value is 2.0 fm, the solid line is for $\Lambda = 0.1$, which gives the optimal energy in Fig. 3, and the dotted line is for $\Lambda = 0.0$. The real parts of Gaussian center parameters for each Slater determinant are common in the two cases, and imaginary parts are just added to the real parts
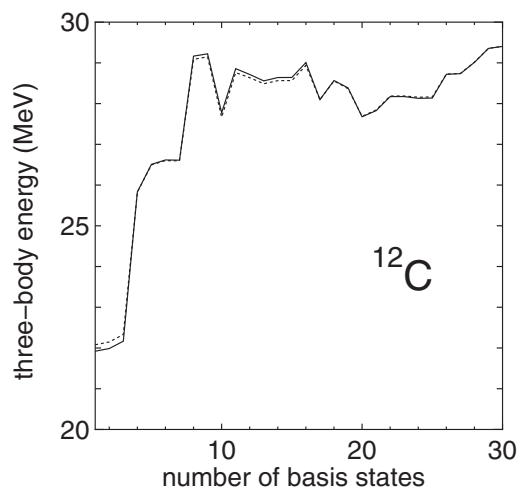
in the $\Lambda = 0.1$ case following Eq. (5). The energies are not converged yet within such a small number of the basis states, but the values of these two lines for the three-body interaction terms are very close and can hardly be distinguished. Indeed, the difference is less than 100 keV. Then we can estimate the contribution of three-body terms in the finite Λ cases by superposing Brink-type Slater determinants ($\Lambda = 0$), where the number of the basis states (N_{max}) is not 30 as in this figure but is increased to 1000.

The absolute value of the elastic form factor ($|F_{(q)}|$) for the 0^+ state of ^{12}C is shown in Fig. 6 as a function of the
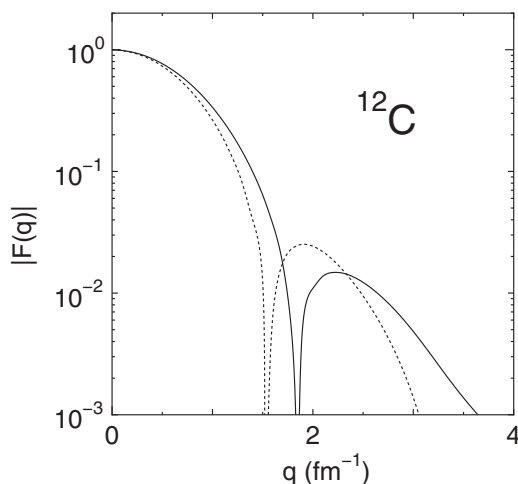

FIG. 6. The absolute value of the elastic form factor ($|F_{(q)}|$) for the 0^+ state of ^{12}C as a function of the momentum transfer q (fm^{-1}). The dotted line is for ($\sigma = 2.0$ fm, $\Lambda = 0.1$), which gives the optimal energy as shown in Fig. 3, and the solid line is the result after mixing the local minimum point (at the limit of $\sigma = 0$ fm, $\Lambda = 0.3$) based on GCM. The experimental values and other theoretical results are compared in Refs. [35,40].

momentum transfer q (fm^{-1}). The dotted line is for ($\sigma = 2.0$ fm, $\Lambda = 0.1$), which gives the lowest energy as shown in Fig. 3. The solid line is the result after mixing the local minimum point (at the limit of $\sigma = 0$ fm, $\Lambda = 0.3$). The mixing ratio of ($\sigma = 2.0$ fm, $\Lambda = 0.1$) and ($\sigma = 0$ fm, $\Lambda = 0.3$) is given by diagonalizing the Hamiltonian matrix based on GCM. The experimental values and other theoretical results are compared in Refs. [35,40]. The dotted line shows the sign change around $q \sim 1.6$ fm^{-1}, which is too small compared with the experiment, reflecting the fact that the ($\sigma = 2.0$ fm, $\Lambda = 0.1$) configuration (the energetically optimal one) has too large spatial extent compared with the experiment (experimentally this sign change occurs around $q \sim 1.8$ fm^{-1}). We have previously mentioned that the mixing of two states, the energy optimal one and the local minimum point with a smaller radius, enables us to reproduce the experimental rms radius, and this mixing turns out to be also important in reproducing the form factor, which is the solid line.

IV. SUMMARY

The THSR wave function has been successfully used for studies of the gaslike nature of α clusters of various nuclei. In this work, we proposed a method to take into account the spin-orbit contribution in THSR by combing it with AQCM. In the standard α cluster models, each α cluster wave function has spin zero because of the spatial symmetry of the α clusters and antisymmetrization effect. Thus the noncentral interactions do not contribute, and this situation is the same in the THSR wave function. The application of a new framework to ^{12}C was presented. The multi-integration in the original THSR wave function was carried out by using a Monte Carlo technique, which is called a Monte Carlo THSR wave function. In ^{12}C, the contribution of the spin-orbit interaction was successfully taken into account. Especially for the cases when the spatial extension is small, the contribution is quite strong, but it decreases with increasing spatial extension. As a result, one local minimum at the limit of zero distance between α clusters and the real minimum state with a sizable α-α distance appear. If we mix these two configurations, we can reproduce the observed matter rms radius. This can be considered as the quantum mechanical mixing of different structures, or, more concretely, the competition of shell and cluster structures.

[1] A. Tohsaki, H. Horiuchi, P. Schuck, and G. Röpke, Phys. Rev. Lett. **87**, 192501 (2001).

[2] Y. Funaki, H. Horiuchi, and A. Tohsaki, Prog. Part. Nucl. Phys. **82**, 78 (2015).

[3] B. Zhou, Y. Funaki, H. Horiuchi, Z. Ren, G. Röpke, P. Schuck, A. Tohsaki, C. Xu, and T. Yamada, Phys. Rev. Lett. **110**, 262501 (2013).

[4] M. Lyu, Z. Ren, B. Zhou, Y. Funaki, H. Horiuchi, G. Röpke, P. Schuck, A. Tohsaki, C. Xu, and T. Yamada, Phys. Rev. C **91**, 014313 (2015).

[5] N. Itagaki, Phys. Rev. C **94**, 064324 (2016).

[6] N. Itagaki, H. Masui, M. Ito, S. Aoyama, and K. Ikeda, Phys. Rev. C **73**, 034310 (2006).

[7] H. Masui and N. Itagaki, Phys. Rev. C **75**, 054309 (2007).

[8] T. Yoshida, N. Itagaki, and T. Otsuka, Phys. Rev. C **79**, 034308 (2009).

[9] N. Itagaki, J. Cseh, and M. Płoszajczak, Phys. Rev. C **83**, 014302 (2011).

[10] T. Suhara, N. Itagaki, J. Cseh, and M. Płoszajczak, Phys. Rev. C **87**, 054334 (2013).

[11] N. Itagaki, H. Matsuno, and T. Suhara, Prog. Theor. Exp. Phys. **2016**, 093D01 (2016).

[12] H. Matsuno, N. Itagaki, T. Ichikawa, Y. Yoshida, and Y. Kanada-Enyo, Prog. Theor. Exp. Phys. **2017**, 063D01 (2017).

[13] H. Matsuno and N. Itagaki, Prog. Theor. Exp. Phys. **2017**, 123D05 (2017).

[14] N. Itagaki and A. Tohsaki, Phys. Rev. C **97**, 014307 (2018).

[15] A. Volkov, Nucl. Phys. **74**, 33 (1965).

[16] T. Ando, K. Ikeda, and A. Tohsaki-Suzuki, Prog. Theor. Phys. **64**, 1608 (1980).

[17] A. Tohsaki, Phys. Rev. C **49**, 1814 (1994).

[18] N. Itagaki, A. Ohnishi, and K. Kato, Prog. Theor. Phys. **94**, 1019 (1995).

[19] N. Itagaki, M. Kimura, C. Kurokawa, M. Ito, and W. von Oertzen, Phys. Rev. C **75**, 037303 (2007).

[20] N. Itagaki, T. Kokalova, M. Ito, M. Kimura, and W. von Oertzen, Phys. Rev. C **77**, 037301 (2008).

[21] N. Itagaki, M. Ito, K. Arai, S. Aoyama, and T. Kokalova, Phys. Rev. C **78**, 017306 (2008).

[22] S. Aoyama and N. Itagaki, Phys. Rev. C **80**, 021304 (2009).

[23] N. Itagaki, T. Kokalova, and W. von Oertzen, Phys. Rev. C **82**, 014312 (2010).

[24] E. Epelbaum, H. Krebs, D. Lee, and Ulf-G. Meißner, Phys. Rev. Lett. **106**, 192501 (2011).

[25] E. Epelbaum, H. Krebs, T. A. Lähde, D. Lee, and Ulf-G. Meißner, Phys. Rev. Lett. **109**, 252501 (2012).

[26] T. Suhara and Y. Kanada-En'yo, Phys. Rev. C **91**, 024315 (2015).

[27] M. Chernykh, H. Feldmeier, T. Neff, P. von Neumann-Cosel, and A. Richter, Phys. Rev. Lett. **98**, 032501 (2007).

[28] M. Chernykh, H. Feldmeier, T. Neff, P. von Neumann-Cosel, and A. Richter, Phys. Rev. Lett. **105**, 022501 (2010).

[29] H. Feldmeier and T. Neff, in *Nuclear Particle Correlations and Cluster Physics*, edited by W. U. Schroeder (World Scientific, Singapore, 2017), p. 71.

[30] T. Neff and H. Feldmeier, J. Phys.: Conf. Ser. **569**, 012062 (2014).

[31] P. Descouvemont and D. Baye, Phys. Rev. C **36**, 54 (1987).

[32] P. Descouvemont, Nucl. Phys. A **709**, 275 (2002).

[33] A. C. Dreyfuss, K. D. Launey, T. Dytrych, J. P. Draayer, and C. Bahri, Phys. Lett. B **727**, 511 (2013).

[34] D. J. Marín-Lámbarri, R. Bijker, M. Freer, M. Gai, T. Kokalova, D. J. Parker, and C. Wheldon, Phys. Rev. Lett. **113**, 012502 (2014).

[35] A. Lovato, S. Gandolfi, R. Butler, J. Carlson, E. Lusk, S. C. Pieper, and R. Schiavilla, Phys. Rev. Lett. **111**, 092501 (2013).

[36] D. M. Brink, in *Many-Body Description of Nuclear Structure and Reactions*, Proceedings of the International School of Physics "Enrico Fermi," Course XXXVI, edited by C. Bloch (Academic, New York, 1966), p. 247.

[37] R. Tamagaki, Prog. Theor. Phys. **39**, 91 (1968).

[38] S. Okabe, Y. Abe, and H. Tanaka, Prog. Theor. Phys. **57**, 866 (1977).

[39] R. Kanungo, W. Horiuchi, G. Hagen, G. R. Jansen, P. Navratil, F. Ameil, J. Atkinson, Y. Ayyad, D. Cortina-Gil, I. Dillmann, A. Estradé, A. Evdokimov, F. Farinon, H. Geissel, G. Guastalla, R. Janik, M. Kimura, R. Knöbel, J. Kurcewicz, Y. A. Litvinov, M. Marta, M. Mostazo, I. Mukha, C. Nociforo, H. J. Ong, S. Pietri, A. Prochazka, C. Scheidenberger, B. Sitar, P. Strmen, Y. Suzuki, M. Takechi, J. Tanaka, I. Tanihata, S. Terashima, J. Vargas, H. Weick, and J. S. Winfield, Phys. Rev. Lett. **117**, 102501 (2016).

[40] Y. Fujiwara, H. Horiuchi, K. Ikeda, M. Kamimura, K. Katō, Y. Suzuki, and E. Uegaki, Prog. Theor. Phys. Suppl. **68**, 29 (1980).